Formation of Formic Acid Derivatives Through Activation and Hydroboration of CO_2 by Low Valent Group 14 (Si, Ge, Sn, Pb) Catalysts

Nery Villegas-Escobar,[†,‡] Henry F. Schaefer III,[*,†] and Alejandro Toro-Labbé[*,‡]

†*Center for Computational Quantum Chemistry, University of Georgia, Athens, Georgia 30602 USA.*

‡*Laboratorio de Química Teórica Computacional (QTC), Facultad de Química, Pontificia Universidad Católica de Chile, Avenida Vicuña Mackenna 4860, Santiago, Chile.*

E-mail: ccq@uga.edu; atola@puc.cl

Abstract

The chemistry of low valent main group elements has attracted much attention in the last decade. The relevance of these species is because they have been able to mimic transition metal behavior in catalytic applications, with decreased material costs and diminished toxicity. In this contribution, we study the L^1EH catalysts (E = Si(II), Ge(II), Sn(II), and Pb(II); L^1=$[ArNC(Me)CHC(Me)NAr]^-$, with Ar=2,6−$iPr_2C_6H_3$) toward the formation of formic acid derivatives through hydroboration of CO_2. A detailed characterization of relevant structures on the potential energy surface enabled us to rationalize different paths for the hydroboration of CO_2. Interestingly, it was found that, according to the activation energies for the whole catalytic cycle, the process of transformation of CO_2 becomes more favored going down in group 14. However, an effective energetic decrease of the process (taking as reference the uncatalyzed reaction between CO_2 and HBpin) is evidenced just from the germanium analog. The trend in reactivity found in the present study is a direct consequence of the change in the central main group element, enabling an enhanced polar character of the **E**–H (L^1EH in the CO_2 activation step) and **E**–O (metal formates in the hydroboration step) as the atomic radii increases. The transient stabilization of reaction intermediates found in the hydroboration step was rationalized through the noncovalent interaction index (NCI) and symmetry-adapted perturbation theory (SAPT). This computational study highlights the reactivity trends in group 14 based hydride catalysts in hydrometallation and posterior hydroboration to form formic acid intermediates. We hope this study will motivate further experimental work in low valent lead chemistry.

Introduction

Most catalytic applications using transition metal (TM) catalysts lead to both excellent yields and turnover frequencies (TOFs). In particular, subtle changes in the ligand, metallic center, or the reaction media can produce gigantic catalytic differences among these catalysts. The problems associated with TM catalysis are the intrinsic toxicity and the elevated cost of synthesis, mainly due to the low abundances in the Earth's crust.[1–3] The main difference of the low valent main group (MG) compounds with the higher valent congeners is that the former have suitable vacancies and/or stereochemically active electron pairs in their electronic structure, and therefore the reactivity of these species can mimic TM chemistry.[4–8] MG elements are often stabilized in their highest oxidation state. Although low valent MG compounds are very reactive, kinetic stability can be gained by the usage of bulky substituents. With this evidence in mind, the usage of the cheaper, more abundant, and (generally) less toxic MG compounds may offer the possibility of substituting the scarcer *d*-block TM catalysts in industrial applications. Interestingly, MG compounds are able to activate small molecules having both unsaturated and strong σ-bonds.[9–31] Activation of small molecules is central to the development of new catalytic systems, since such activation is a fundamental step in most catalytic cycles.

Carbon dioxide is one of the primary sources of greenhouse gases and mainly responsible for global warming. Although reducing its high concentrations in the air may be impractical, the use of this gas as C1 feedstock for the production of added-value compounds such as formic acid, methane, formaldehyde, and methanol is promising.[32–37] Germanium(II)- and tin(II)-based catalyst have been proven to be able to carry out hydrometallation reactions of carbonyl-containing compounds including CO_2.[13,14,38–41] Hydrometallation of polar and nonpolar unsaturated bonds has great impact in both organic and inorganic synthesis.[42–47] In this research, we have centered our attention in the hydroboration of CO_2 for potential formation of formic acid by group 14 MG catalysts.

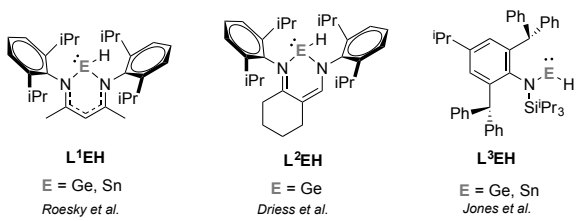

Figure 1: Relevant low valent Ge and Sn compounds.

Roesky *et al.* synthetized Ge(II) and Sn(II) hydride catalysts using the bidentate N-arylisopropylβ-diketiminate ligand (L^1EH in Figure 1) which showed a great reactivity toward CO_2 activation in toluene at room temperature.[13–15] It has been shown both experimentally and computationally that the CO_2 activation reaction becomes more favored as the metal size increases.[13–15,48] Interestingly, the reaction of complexes L^1GeH and L^1SnH cleanly reacts toward CO_2 activation without the use of any cocatalyst to afford the respective formates $L^1EOC(O)H$ (E = Ge, Sn).[13–15] Following this stage, a hydride source is needed to restore the catalyst. Although reduction of CO_2 by B–H bonds and without a catalyst can be traced from the 1950s,[49,50] hydroboration of CO_2 with even the most reactive BH_3 adducts is carried out in presence of a catalyst.[51–60] Reaction of $L^1GeOC(O)H$ with lithium aminoborane (LiH_2NBH_3) in THF at room temperature restores **2** and yield lithium

formate LiOC(O)H in quantitative yield.[39] Treatment of LiOC(O)H with HCl easily produces produces formic acid. Moreover, the reaction 1:1 of L^1GeOC(O)H and H_3NBH_3 can also be carried out, but higher temperature is needed, most probably due to the low solubility of H_3NBH_3.[39] Interestingly, the same reaction using three eq. of H_3NBH_3 gives the corresponding methanol derivate (H_3NH_2BOMe), that posterior workup with deuterated water produces MeOD.[39] Driess *et al.* used complexes L^1GeH and L^2GeH (Figure 1) for the reaction with CO_2 giving the corresponding germylene formates, which after reaction with three eq. AlH_3NMe_3 and workup with water gave methanol. Interestingly, formation formic acid was not reported by the authors.[35] Jones *et al.* synthetized L^3GeH and L^3SnH (Figure 1). In a first study, these compound were used to hydroborate ketones with HBpin.[36] It is worth noting that reactions with the tin-analogues were much faster than the reactions with the germanium-based complex, which may give hints of trends in reactivity along group 14. Later on, L^3GeH and L^3SnH were used for reduction of CO_2 to methanol equivalents with impressive turnover frequencies.[37] Computations performed in that study concluded that hydroboration of the formate L^3GeOC(O)H to HCOOBpin corresponded to a dead end of the reaction toward the desired formation of the methanol intermediates. Computationally, Takagi and Sakaki[61] proposed the use of SiF_3H as hydride-source with L^1GeOC(O)H to restore the catalyst yielding $HCOOSiF_3$. To our knowledge, computational characterization for the hydroboration of CO_2 using L^1EH and HBpin has not been attempted for group 14 elements (E = Si, Ge, Sn, and Pb).

In this research, we shed light on the mechanism for the hydroboration of CO_2 by L^1GeH (E = Si, Ge, Sn, and Pb) toward the formation of the formic acid derivative HCOOBpin. The whole catalytic cycle (Figure 2) has been computed for each catalyst using density functional theory (DFT). Our intention in this contribution is to study a possible periodic trend in reactivity along the group 14 catalysts, together with a complete characterization of reactions intermediates and conformers that can be obtained in the potential energy surface for this particular reaction. Characterization of reactive reaction intermediates for the hydroboration step was studied in detail to comprehend the type of interactions that rule the transient viability of these species.

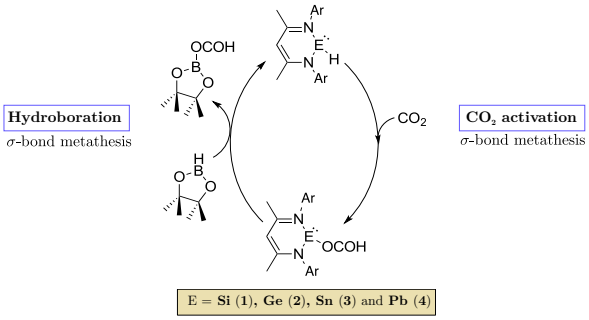

Figure 2: Catalytic cycle for the hydroboration of CO_2. Labelling for catalysts is also shown.

Theoretical Methods

The activation and hydroboration of CO_2 were studied using density functional theory (DFT) methods. Optimization of minima and transition states (TSs) were carried out using the well-tested hybrid meta-GGA M06–2X functional[62] together with the 6-31G(d, p) basis set.[63,64] This level of theory was selected since it has been proposed as a reliable methodology for

main group chemistry for both thermodynamics and kinetic energies without compromising long computational times and accuracy.[62,65,66] Main Group 14 elements (Si, Ge, Sn, and Pb) were modeled using the LANL2DZ basis, which includes quasi-relativistic effective core potentials.[67] Nature of each species was confirmed by frequency computations using analytic second derivatives of the energy with respect to the atomic coordinates.[68] TSs were found through initial relaxed surface scans on the potential energy surface and definitively refined by geometry optimizations. Verification of transition states was confirmed by inspection of a single imaginary vibrational mode and then connected with reactants and products by employing the intrinsic reaction coordinate (IRC) procedure.[69–71]

Due to significant errors are obtained when the harmonic approximation is used to compute thermochemical quantities for low-frequency modes, the quasi-Rigid Rotor Harmonic Oscillator (quasi-RRHO) method introduced by Grimme has been employed.[72] After the free energy correction is obtained, Gibbs free energies are computed as:

$$\Delta G = \Delta E + \Delta G^{T}_{RRHO} + \Delta\delta G^{T}_{solv}(X) \quad (1)$$

where ΔE corresponds to the gas phase electronic energy difference, ΔG^{T}_{RRHO} collects the Gibbs free energy correction with zero-point vibrational energies, and $\Delta\delta G^{T}_{solv}(X)$ accounts for solvation energy. The $\Delta\delta G^{T}_{solv}(X)$ term was computed using toluene as solvent through the polarizable continuum model (PCM)[73] through single-point computations on the already optimized gas-phase geometries.

All computations were performed in the Gaussian09 software package.[74] Bonding and charge analyses were carried out through the NBO program[75] interfaced with Gaussian09.

In order to qualitative characterize noncovalent interactions, the NCIplot program was used.[76,77] However, for a quantitative analysis of noncovalent interactions of relevant structures, symmetry-adapted perturbation theory (SAPT)[78] was used. Quantification of charge transfer effects were computed through SAPT-CT approach.[79–82] SAPT0/cc-pVDZ computations where carried out in Psi4.[83] Specifically, DF–SAPT0[84,85] was used in all computations with the cc-pVDZ-ri basis set.

Results and Discussion

In a first contribution,[48] the CO_2 activation step was studied in great detail. It was found that the σ-bond metathesis reaction for the incorporation of CO_2 into the **E**–H bond is favored as the size of the MG element increases. As the central MG element increases in size, a larger charge separation appears in the **E**–H bond, facilitating the insertion of CO_2 into this bond. Moreover, it was found that two approaching modes of CO_2 to the **E**–H bond can take place: the front- (**R1**) and back-side (**R1**) approaches (see Figure 3(a)). It was found the **R1** and **R2** reaction channels give different formate stereoisomers, $\mathbf{P}_{\mathbf{E}\mathrm{H}i}$ and $\mathbf{P}_{\mathbf{E}\mathrm{H}o}$, respectively (see Figure 3(b)). Notation of products stand for the spatial orientation of the hydrogen in the formate complex: in $\mathbf{P}_{\mathbf{E}\mathrm{H}i}$ the hydrogen atom is pointing toward the NacNac ligand while in $\mathbf{P}_{\mathbf{E}\mathrm{H}i}$ the hydrogen atom is located outward with respect to the complex (see Figure 3(b) for reference). Although rotation of the **E**–O bond is unable to interconvert between both reaction products ($\mathbf{P}_{\mathbf{E}\mathrm{H}i}$ and $\mathbf{P}_{\mathbf{E}\mathrm{H}o}$), combination of the C–O and **E**–

O bond rotations can produce even more stable reaction products: $\mathbf{P_{EO}}_{i}$ and $\mathbf{P_{EO}}_{o}$ (for details the reader is referred to reference[48]). The whole set of reaction products are schematized in Figure 3(b).

In this work, we focus our attention

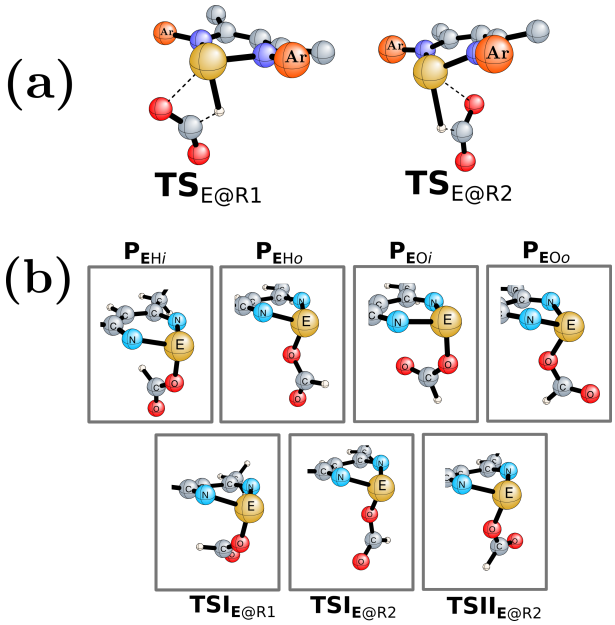

Figure 3: (a) Different approaches (**R1** and **R2**) of CO_2 towards the **E**–H bond. (b) Different formate conformers and respective transition state structures.

on the study of the full catalytic cycle for the hydroboration of CO_2. As for the CO_2 activation step, the hydroboration mechanism takes place under a σ-bond metathesis regime (Figure 2). This is a key step because it encompasses the recovery of the catalyst and the formation of the dioxaborolane formate (HCOOBpin) as product.

From the conformational analysis performed in ref.,[48] it is clear that for the hydroboration step, the approach of HBpin has to be studied for each of the conformers found: $\mathbf{P_{EH}}_{i}$, $\mathbf{P_{EH}}_{o}$, $\mathbf{P_{EO}}_{i}$ and $\mathbf{P_{EO}}_{o}$ (see Figure 3 (b)).

For $\mathbf{P_{EH}}_{i}$ and $\mathbf{P_{EO}}_{i}$ formates, the HBpin attack should come by the front-side (facing the **E**–O bond) in order to carry out the $\sigma-$bond metathesis reaction. However, due to strong steric repulsions among the methyl groups in HBpin and the *i*Pr groups in the NacNac ligand, the σ-bond metathesis is not possible, as shown in Figure 4. In contrast to this, to prove that the steric repulsions are responsible for the non-occurrence of this reaction pathway, methyl groups in HBpin and in the L^1 backbone were interchanged by hydrogens, in which a proper TS structure is successfully found (right side Figure 4). Although a collection of transition states was found with the non-methylated HBpin reagent, these are not considered in the present study. Thus, for the hydroboration step, only reaction pathways of both $\mathbf{P_{EH}}_{o}$ and $\mathbf{P_{EO}}_{o}$ formates with HBpin were considered.

Analysis of Reaction Pathways

In this section, results and discussions regarding the full catalytic cycle for the hydroboration of CO_2 through the innovative use of low valent MG catalysts are presented (Figure 2). The uncatalized reaction between HBpin and CO_2 is presented in Figure 5. The whole catalytic cycles for Si(II), Ge(II), Sn(II), and Pb(II) catalysts are shown in Figures 6, 7, 9 and 10, respectively. For all energy profiles, key structures are shown. Furthermore, the activation, conformation and hydroboration steps were labeled along the energy profile in order to have a complete characterization of the PES.

The catalytic cycle starts with the formation of a reactive complex between the NacNacEH complex and CO_2. The stabilization of the reactant complex is due to long-range interactions, which promote stabilization through non-covalent interac-

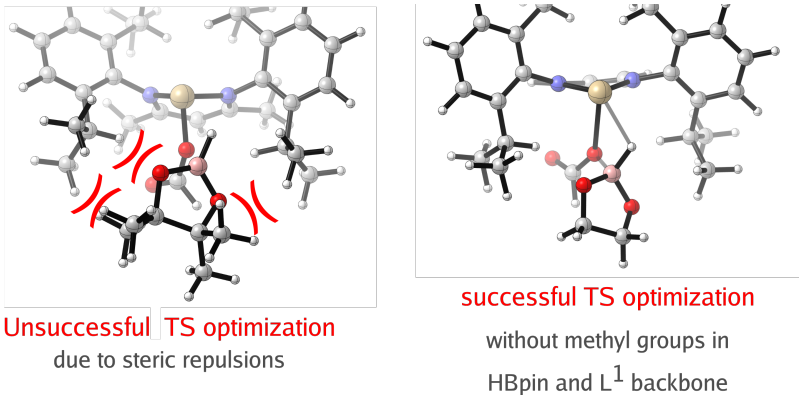

Figure 4: Schematic representation of steric repulsions in **P**E**O**i + HBpin system (left) and TS structure for the non-methylated HBpin with **P**E**O**i (right).

tions. SAPT0 computations suggest that stabilization of the reactant complex is favored through electrostatic and dispersion interactions, with the electrostatic component being more predominant. Due to the separation of the reacting species ($\sim$ 2.5 Å on average, taking into account the **E**–H$\cdots$CO$_2$ interaction), favored induction effects are less pronounced. After the reaction complex is formed, the CO$_2$ activation takes place, obeying a σ-bond metathesis regime by the formation of a four-membered transition state (see Figure 3(a)). As the σ-bond metathesis mechanism takes place, the dispersion component remains steady compared to a sharp stabilization of the reacting species driven by electrostatic interactions at the TS vicinity. Accordingly, the induction (polarization + charge transfer) term, which is close to zero at the reactant complex, becomes the most favorable interaction at the TS structure (see Figures S3 and S4 in Supporting Information). As mentioned above, the approach of CO$_2$ to the **E**–H bond can be carried out by means of the **R1** and **R2** reaction pathways (see Figure 3(a) for reference). In an earlier contribution, we studied in detail the CO$_2$ activation mechanism, as well as the conformational step involving a combination of **E**–O and C–O torsions. The reader is referred to reference[48] for further reading.

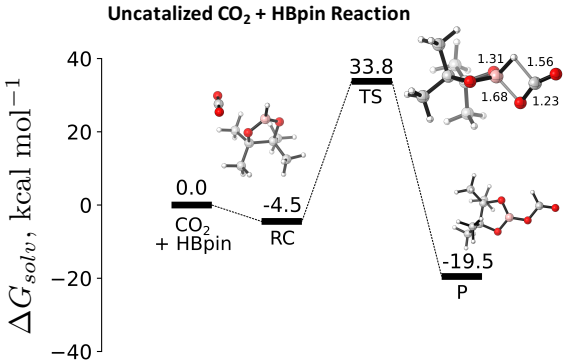

Figure 5: Energy profile for the reaction between CO$_2$ and HBpin. Gibbs free energies in toluene are reported in kcal mol^{-1}.

For comparison purposes, the uncatalized HBpin+CO$_2$ reaction has been computed and shown in Figure 5. The reaction takes place under a one-step regime, through a four-membered TS. Due to the relative stability, ease of synthesis, and high selectivities, HBpin and HBcat (cat = 1,2$-$O$_2$C$_6$H$_4$) have emerged as candidates of the family of the dioxalborolanes.

Table 1: Activation energies for CO_2 activation ($\Delta G^{\ddagger}_{CO_2}$) and hydroboration ($\Delta G^{\ddagger}_{\mathrm{LA}}$, $\Delta G^{\ddagger}_{Hydrob.}$, and $\Delta G^{\ddagger}_{HB}$) . $\Delta G^{\ddagger}_{total}$ represents the total activation energy for the whole catalytic cycle from reactants to products in the forward direction. Gibbs free energies in toluene are reported in kcal mol^{-1}.

uncatalyzed reaction							
HBpin+CO_2	$\Delta G^{\ddagger}$ = 38.3 kcal mol^{-1}		ΔG° = −15.0 kcal mol^{-1}				
catalyzed reaction							
MG	Path	$\Delta G^{\ddagger}_{CO_2}$	**Product**	$\Delta G^{\ddagger}_{\mathrm{LA}}$	$\Delta G^{\ddagger}_{Hydrob.}$	$\Delta G^{\ddagger}_{HB}$	$\Delta G^{\ddagger}_{total}$
Si	**Si-R1/Oo**	21.0	$\mathbf{P}_{1Oo}$	···	23.3	···	50.0
Si	**Si-R2/Ho**	21.8	$\mathbf{P}_{1Ho}$	···	22.3	···	44.3
Ge	**Ge-R1/Oo**	15.7	$\mathbf{P}_{2Oo}$	7.9	8.5	0.7	36.7
Ge	**Ge-R2/Ho**	21.2	$\mathbf{P}_{2Ho}$	···	19.5	···	40.7
Sn	**Sn-R1/Oo**	12.2	$\mathbf{P}_{3Oo}$	3.3	4.8	0.6	23.1
Sn	**Sn-R2/Ho**	14.7	$\mathbf{P}_{3Ho}$	···	15.0	0.6	30.3
Pb	**Pb-R1/Oo**	7.9	$\mathbf{P}_{4Oo}$	4.7	0.6	0.8	17.8
Pb	**Pb-R2/Ho**	6.5	$\mathbf{P}_{4Ho}$	5.0	3.9	1.2	15.8

However, high temperatures are frequently required which promote decomposition of the borane, into BH_3-like intermediates, resulting in several organoborane products.[86] Activation and reaction free energies (taking as reference the reactant complex) were found to be 38.3 and -15.0 kcal mol^{-1}, respectively. The high activation barrier of this reaction explains why its realization under mild reaction conditions is challenging. The magnitude of the activation energy for this transformation (and the $\sigma-$bond metathesis reactions studied in this work) is high because they take place under a highly constrained four-membered TS and therefore the use of a catalyst is mandatory. Gibbs free energy for the uncatalyzed and catalyzed reactions are reported in Table 1. Reaction pathways are represented by **E-Ri/Ho** and **E-Ri/Oo** (**E** = **Si**, **Ge**, **Sn**, and **Pb**; **i** = **1** or **2**; **Ho** and **Oo** follow the spatiality of the formate).

The whole catalytic cycle for the silicon derivative, the lightest MG element in the studied series, is shown in Figure 6. Although the NacNacSiH has not been prepared yet, derivatives stabilized by TM compounds have been reported.[87,88] Activation free energies for the incorporation of CO_2 into the **E**–H bond were found to be 21.0 and 21.8 kcal mol^{-1} for the **R1** and **R2** paths, respectively. After the conformational step it can be seen that formation of the reactive complexes $\mathbf{P}_{1Oo}$+HBpin and $\mathbf{P}_{1Ho}$+HBpin are favored thermodynamically with ΔG° values of −27.7 and −27.8 kcal mol^{-1}, respectively. For the hydroboration step, a single TS is observed for both reaction pathways. Structures for the hydroboration step are represented by E–Ho or E–Oo in subscript (E = 1 (Si), 2 (Ge), 3 (Sn) and 4 (Pb); Ho and Oo follow the spatiality of the formate). Accordingly, transition states are labeled as $\mathbf{TSIII}_{\text{E-Ho}}$ and $\mathbf{TSIII}_{\text{E-Oo}}$ for $\mathbf{P}_{EHo}$ and $\mathbf{P}_{EOo}$ formates, respectively. A four-membered ring characterizes the main TS structure for the hydroboration step (**E**–O–B–H), which includes the formation of the **E**–H and B–O

bonds and the breaking of the **E**–O and B–H bonds. Gibbs free energies of activation, computed taking as reference the reactant complex between the formate and HBpin for the Oo and Ho pathways, are very close to each other, 23.3 and 22.3 kcal mol^{-1}, respectively. This result suggests that a more likely path cannot be established, and thus both pathways are expected to take place. Furthermore, it is worth noting that the activation barriers for the hydroboration step are also close to that of the corresponding CO_2 activation step. Bond distances within the four-membered ring at the TS structures are quite similar when comparing the two reaction paths, with discrepancies of only 0.01 Å on average. It is worth noting that the activation energy for the whole activation free energy for the catalytic cycle is higher than the uncatalized reaction between HBpin and CO_2. The reason is due to the large dissociation energies (D°_{298}) of the Si–H (in complex **1**) and Si–O (in $\mathbf{P}_{1Ho}$ and $\mathbf{P}_{1Oo}$) bonds, 70.1 kcal mol^{-1} and 191.1 kcal mol^{-1}, respectively.[?] Overall, considering the appearance of a relatively high activation barrier for both the CO_2 activation and hydroboration steps, the reaction may be possible but less likely to take place at room temperature and to use low pressures of CO_2.

In the case of the experimentally available Ge(II) based complex,[13,15] activation free energies of 15.7 and 21.2 kcal mol^{-1} were obtained for the **R1** and **R2** reaction paths in the CO_2 activation step. The hydroboration of CO_2 is thought to be a stoichiometric 1:1:1 reaction in CO_2, catalyst, and HBpin, respectively. Interstingly, Jones *et al.*[36] reported no noticeable reactions between L^{3}GeH or L^{3}SnH hydride with HBpin, as a result of favorable acid-base Lewis interactions. It was observed that the particular low field hydride resonance (^{1}H NMR) of the complexes is only negligibly shifted after addition of HBpin to the solution containing the catalyst. We studied the Lewis acid-base interaction between **2** and HBpin, and we have found that the lone pair over Ge(II) and Sn(II) is sterically protected from reacting with the empty *p*-orbital on the boron atom. Interestingly, the hydroboration step for the germanium analog shows noticeable differences between the Ho and Oo reaction pathways (Figure 7). As for silicon, the Ho reaction channel exhibit a single TS for the hydroboration of CO_2 with an activation free energy of 19.5 kcal mol^{-1}. On the other hand, the Oo pathway is carried out under a multistep regime. First, as HBpin approaches the formate complex, a favorable B$\cdots$O interaction takes place, giving rise to the formation of a Lewis Adduct (LA) intermediate ($\mathbf{INT}^{\mathrm{LA}}_{\text{2-Oo}}$) with an activation free energy of 7.9 kcal mol^{-1}. The $\mathbf{INT}^{\mathrm{LA}}_{\text{2-Oo}}$ system is formed with a B–O distance of 1.68 Å (bond order 0.47). Once the LA intermediate is formed, formation of the Ge–H bond and breaking of the Ge–O bond start to take place, giving rise to $\mathbf{TSIII}_{\text{2-Oo}}$. From the appearance of $\mathbf{INT}^{\mathrm{LA}}_{\text{2-Oo}}$ to the formation of $\mathbf{TSIII}_{\text{2-Oo}}$, the strengthening of the B–O bond and the weakening of the B–H and Ge–O bonds take place. At $\mathbf{TSIII}_{\text{2-Oo}}$ the B–O distance is decreased from 1.68 (in $\mathbf{INT}^{\mathrm{LA}}_{\text{2-Oo}}$) to 1.55 Å (89% of formation with respect to the product structure). The Gibbs free energy of activation from the LA intermediate to the rate-limiting TS structure is just 8.5 kcal mol^{-1}. For this path, the activation barrier of the whole hydroboration process, which can be considered as the sum of $\Delta G^{\ddagger}_{\mathrm{LA}}$ and $\Delta G^{\ddagger}_{Hydrob.}$, is 16.4 kcal mol^{-1}, which is more favored compared with the concerted Ho path (19.5 kcal mol^{-1}). Interestingly, the B–H bond does not change considerably

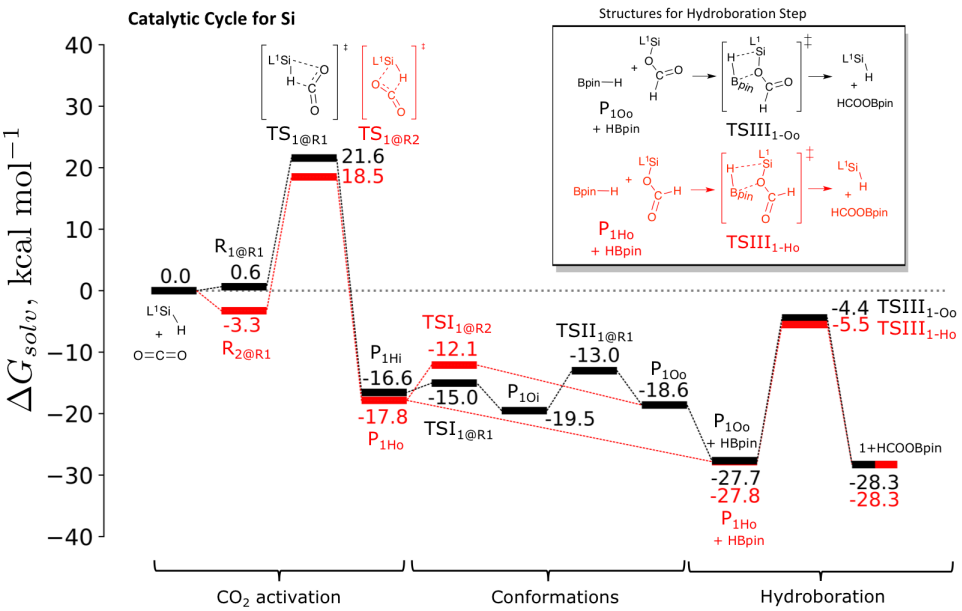

Figure 6: Gibbs energy profile for the catalytic hydroboration of CO_2 by the low valent Si catalyst (**1**). **Si-R1/Oo** and **Si-R2/Ho** pathways are represented in black and red, respectively. Energies are reported in kcal mol^{-1} using toluene as solvent.

from $\mathbf{INT}^{\mathrm{LA}}_{\text{2-Oo}}$ to $\mathbf{TSIII}_{\text{2-Oo}}$. Afterward, the Ge–O bond is broken, and a favorable Ge$\cdots$H$\cdots$B cooperative interaction gives rise to a reactive H-bridged intermediate $\mathbf{INT}_{\text{2-Oo}}$. At $\mathbf{INT}_{\text{2-Oo}}$, the Ge$\cdots$H$\cdots$B interaction corresponds to a three-center two-electron (3c–2e) interaction. In the $\mathbf{INT}_{\text{2-Oo}}$ species, the Ge–H and B–H bond distances are 1.75 and 1.45 Å, respectively. Special attention to $\mathbf{INT}^{\mathrm{LA}}_{\text{2-Oo}}$ and $\mathbf{INT}_{\text{2-Oo}}$ intermediates will be given later in this work. Moreover, it is worth to note that the low activation free energies of $\mathbf{TSII}^{\mathrm{LA}}_{\text{2-Oo}}$ and $\mathbf{TS}_{\text{2-Oo}}$ toward $\mathbf{P}_{\mathrm{E}}\mathrm{O}_{o}$ + HBpin and **2** + HCOOBpin, respectively, are visualized as shoulders appearing in the PES.

In a mixed experimental-computational study, Maron and Jones *at al.* reported the use of L^{3}GeH and L^{3}SnH hydrides for the reduction of CO_2 to methanol equivalents (MeOBR$_2$) by using HBpin or HBcat as hydride source.[37] DFT computations proved that a respective μ-bridge intermediate is formed with activation energies close to 1 kcal mol^{-1}, recovering the catalyst and giving HCOOBpin. Instead of a 4-membered TS as reported here, they proposed a 6-membered TS. In Figure 8, a summary of the reactions using L^{1}GeH and L^{3}GeH with representation of the respective TSs is presented and used for discussion. Through the formation of the 6-membered TS, the authors[37] reported a low activation enthalpy of 2.2 kcal mol^{-1} compared to a larger activation free energy reported in the present contribution of 16.4 kcal mol^{-1}. This energetic difference reveals a big difference in structure-reactivity differences between mono- and bidentate ligands. Motivated by the results of Maron and Jones, we studied the occurrence of the 4- and 6-membered TS using L^{1}GeH and L^{3}GeH. We found that the catalyst's design prevents the forma-

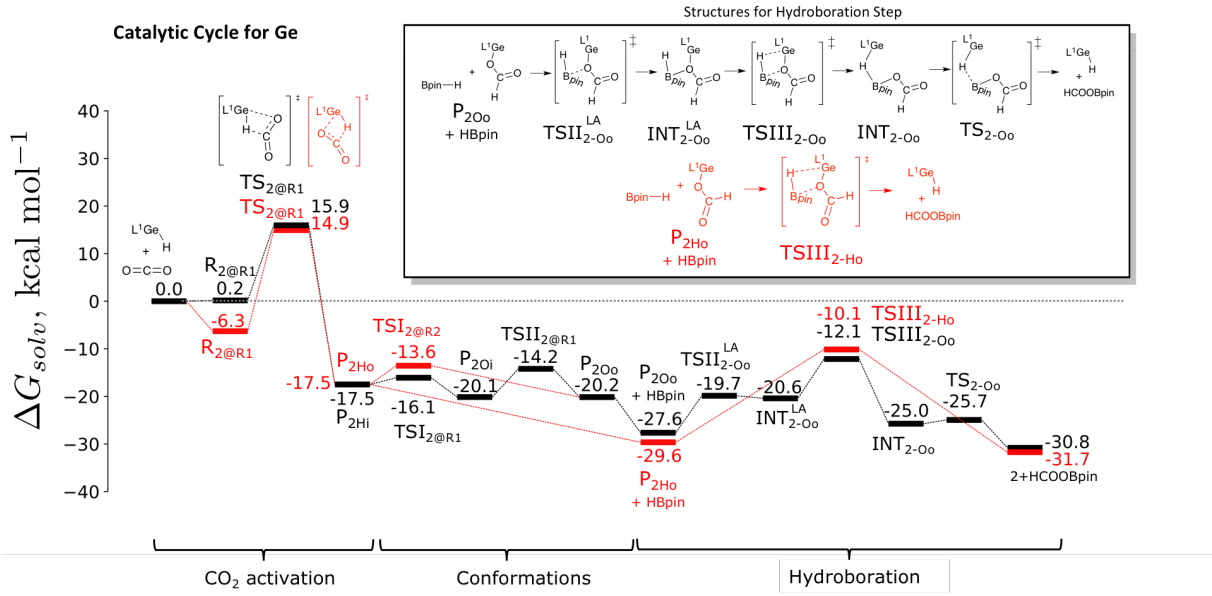

Figure 7: Gibbs energy profile for the catalytic hydroboration of CO_2 by the low valent Ge catalyst (**2**). **Ge-R1/Oo** and **Ge-R2/Ho** pathways are represented in black and red, respectively. Energies are reported in kcal mol^{-1} using toluene as solvent.

tion of a 6-membered (4-membered) TS when the L^{1}GeH (L^{3}GeH) catalyst is used. Let us define the position of the formate (–OCOH) unit as the *front-side*. For the L^{1}GeH complex a 6-membered TS is not possible due to the bidentate ligand retains the Ge atom in position. Thus the Ge–O–C angle in the formate complex prevents its change as the 6-membered formation comes into effect (the bidentate ligand firmly maintains the pyramidal geometry in Ge; see **P**2O$_o$ in Figure 4(b) for reference). Furthermore, the bulkiness of both the HBpin and ^{i}Pr groups in the NacNac ligand also helps prevent the 6-membered TS. Regarding the L^{3}GeH catalyst, it is clear from Figure 8(b) that the *back-side* approach is blocked by the $-CH(Ph)_2$ and $-SiPr_3$ moieties in the L^3 ligand.

According to Maron and Jones,[37] after the formic acid-derivative is formed, HCOOBpin reacts again with the L^{3}GeH and in several stages using 2 more equivalents of HBpin to yield the methanol derivative CH_3OBpin and $(Bpin)_2O$ (Figure 8(b)). The reaction of L^{1}GeH toward the formation of methanol derivatives with HBpin is under active research in our group. We believe that a control in the selectivity toward formic acid, formaldehyde, and methanol equivalents can be done by means of changes in stoichiometry, identity (bulkiness or reductant strenght) of the hydride-source, the nature (steric demand and denticity) and catalytic loadings of the catalyst as previosly reported for Ni and Pd catalysts.[89]

In summary, the formation of formic-acid or methanol derivatives with Ge(II) hydrides (and extended to other catalysts) is subject to the stoichiometry of the reaction. Moreover, it can be concluded that the denticity and bulkiness of the ligand establish the appearance of a 4- or 6-membered TS.

On the other hand, the experimentally

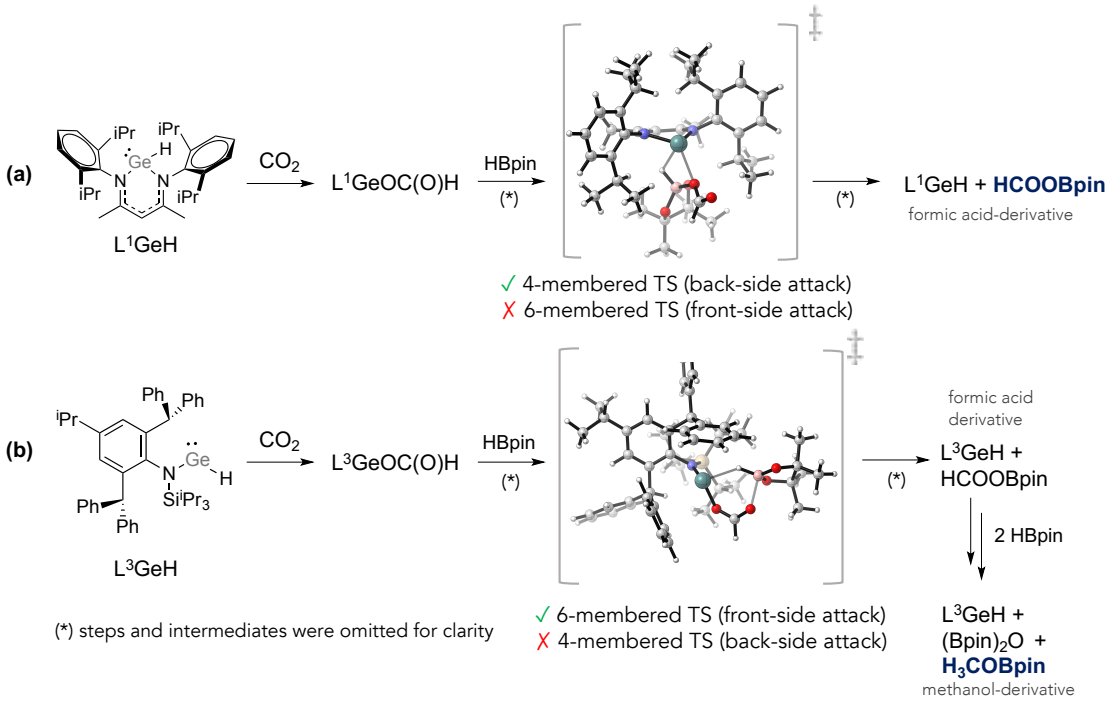

Figure 8: Schematic representation for the hydroboration of CO_2 using (a) L^1GeH and (b) L^3GeH. Transition state structures for the hydroboration step for both catalysts are also shown.

obtained tin-containing complex[14,15] can reduce even more the activation energy for the CO_2 capture, as the Sn–H bond becomes more polarizable than the Ge analog.[48] Gibbs free energies of activation for the reaction pathways, **R1** and **R2**, are very close, namely 12.2 and 14.7 kcal mol^{-1}, respectively. As may be noticed, activation energies involving complex **3** are lower than that obtained for complex **2**, thus attributing faster conversion when using tin-derivatives than germanium, as observed experimentally.[36,37] With regard of the hydroboration step, it can be seen that the same mechanism for the lighter Ge$^{(II)}$ congener takes place on the Oo pathway, but different to that for the Ho path. For tin, the Ho pathway does not exhibit the formation of the Lewis adduct, $\mathbf{INT}^{LA}_{3\text{-Oo}}$. For both pathways, formation of the Sn–H bond and breakage of the Sn–O bond through the $\mathbf{TSIII}_{3\text{-Ho}}$ ($\Delta G^{\ddagger}$ = 15.0 kcal mol^{-1}) and $\mathbf{TSIII}_{3\text{-Oo}}$ species ($\Delta G^{\ddagger}$ = 8.1 kcal mol^{-1} from the reactive complex and 4.8 kcal mol^{-1} from the Lewis Adduct) dominates the hydroboration step. As may be observed from Figure 9, the Oo pathway is energetically more favored than the Ho pathway through the formation of the reaction intermediates.

Finally, the most reactive complex for both activation and hydroboration of CO_2 is the computationally proposed NacNacPbH catalyst. The lead β-diketiminate halide,[90] aryloxyde,[91] phosphanide,[92] alcoxide,[92–94] alkyl,[95] amido,[94,96] anilido,[96] among other derivatives, have been prepared, but complex **3** has not been obtained to date. Recently, efforts made by the groups of Wasserman and Power have shown the first low valent lead hydride compounds using monodentated lig-

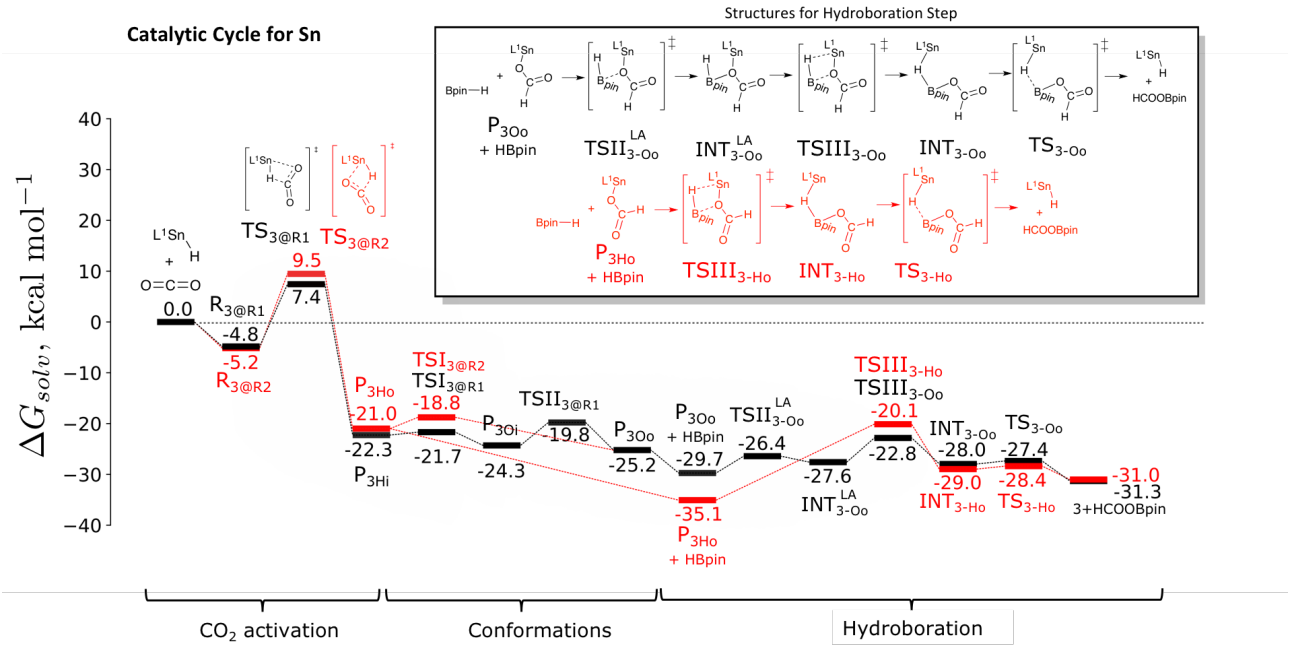

Figure 9: Gibbs energy profile for the catalytic hydroboration of CO_2 by the low valent Sn catalyst (**3**). **Sn-R1/Oo** and **Sn-R2/Ho** pathways are represented in black and red, respectively. Energies are reported in kcal mol^{-1} using toluene as solvent.

ands.[97,98] Activation energies for the CO_2 activation step are 7.9 and 6.5 kcal mol^{-1} for **R1** and **R2**, respectively. In the hydroboration step, both reaction pathways exhibit the formation of the LA and H-bridged intermediates that promote a more feasible way for the transformation of CO_2. For the Ho pathway, the activation energy involving $\mathbf{TSIII}_{4\text{-Ho}}$ amounts to 8.9 kcal mol^{-1} ($\Delta G^{\ddagger}_{\text{LA}} + \Delta G^{\ddagger}_{Hydrob.}$). Furthermore, for the Oo path the total activation energy involving $\mathbf{TSIII}_{4\text{-Oo}}$ is even lower with 5.3 kcal mol^{-1}.

Activation energies for the σ-bond metathesis in the activation and hydroboration of CO_2 from Ge to Pb were found to be low enough –below 22 kcal mol^{-1}– and therefore the process is highly feasible to take place under mild reactions conditions. For comparison purposes, the free activation energy of 38.3 kcal mol^{-1} for the uncatalyzed CO_2+HBpin reaction is compared to the sum of the activation energies of the individual processes in the forward direction ($\Delta G^{\ddagger}_{total}$). The latter energies are collected in Table 1. As it was observed from the energy profiles for each catalyst, there is a noticeable decrease in the activation energies for each stage concerning the uncatalyzed reaction. However, taking the total activation energies for each catalytic cycle, it can be seen that a sufficient reduction of the total activation energy, $\Delta G^{\ddagger}_{total}$, is observed from the germanium analog (only Oo pathway) being more favored going down in group 14 (both reaction pathways). More interestingly, the lead-derived complex **4** can decrease the total energy barrier less than one-half when compared to the uncatalyzed reaction.

In Summary, we have shown evidence that the catalytic process becomes more effective with regards to activation ener-

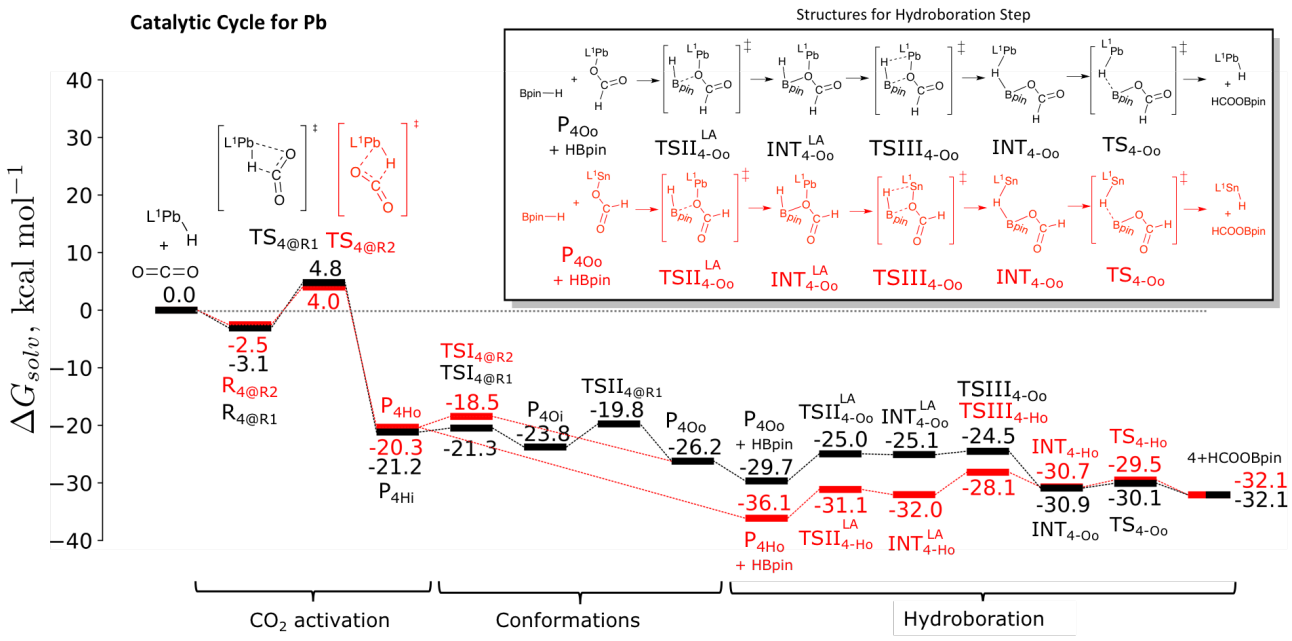

Figure 10: Gibbs energy profile for the catalytic hydroboration of CO_2 by the low valent Si catalyst (**4**). **Pb-R1/Oo** and **Pb-R2/Ho** pathways are represented in black and red, respectively. Energies are reported in kcal mol^{-1} using toluene as solvent.

gies as we move down group 14, in which an apparent decrease (compared to the uncatalyzed reaction) of the activation energy can be observed just from the germanium derivative **2**. Moreover, from these results, it is concluded that the decrease of the activation energies is directly attributed to the effect of the central low valent group 14 element. It was also found that steric demand and denticity of the ligand can determine the type of TS (4- or 6-membered TSs) in the hydroboration step.

Reaction Intermediates: $\mathbf{INT^{LA}_{2\text{-}Oo}}$ and $\mathbf{INT_{2\text{-}Oo}}$

In this section, the germanium reaction intermediates $\mathbf{INT^{LA}_{2\text{-}Oo}}$ and $\mathbf{INT_{2\text{-}Oo}}$ were chosen as representatives of the whole set of group 14 intermediates. Bonding features, as well as interactions that lead to the formation of the LA and H-bridged intermediates, are studied in great detail.

First, to corroborate the appearance of the reaction intermediates and to assure that they were not obtained as an artifact of the density functional used in the present work, a benchmark study was done (see Table S1 in Supporting Information). Over 20 DFT functionals were used, encompassing pure, hybrid, hybrid meta-GGA and long-range corrected functionals. Interestingly, it was found that geometry optimizations performed with functionals that do not include dispersion corrections are not able to reproduce both $\mathbf{INT^{LA}_{2\text{-}Oo}}$ and $\mathbf{INT_{2\text{-}Oo}}$, yielding the reactive complex (**P2**o_o + HBpin) or the product structure (**2** + HCOOBpin), respectively. Clear examples of the latter findings are the ones computed with B3LYP and APF functionals that converged to the

desired intermediates once the dispersion correction is taken into account through the dispersion corrected version, B3LYP-D3BJ and APFD, respectively. On the other hand, most of Minnesota functionals can reproduce both reaction intermediates. Therefore, the inclusion of dispersion corrections are necessary to have a full characterization of relevant structures along with the reaction mechanism.

As mentioned above, the LA-intermediate is formed from the interaction of the Lewis acidic boron atom of HBpin and the oxygen atom in the formate complex. The H-bridged intermediate instead is formed from the cooperative 3c–2e Ge$\cdots$H$\cdots$B attractive interaction. As $\mathbf{INT}_{\text{2-Oo}}$ exhibits the Ge$\cdots$H$\cdots$B interaction, both B–H breaking and Ge–H bond-breaking reaction paths were studied. In Figure 11, the two reaction paths are depicted along with relevant structures. If the B–H bond in $\mathbf{INT}_{\text{2-Oo}}$ breaks, a low activation energy allows the formation of the desired reaction products: **2** + HCOOBpin (neutral path, Figure 11(a)). On the contrary, if the Ge–H bond breaks, it would lead to the formation of ionic species (ionic path, Figure 11(b)). Undoubtedly, the neutral path is preferred. In the ionic path (Figure 11 (b)), as the Ge–H bond distance increases, the energy does so almost linearly. At $d_{\text{Ge–H}} = 3.96$ Å ($\Delta E = 23.9$ kcal mol^{-1}) convergence problems arise as the charged species are far apart. However, this is enough evidence to conclude that there is no competition among the neutral and ionic paths. Therefore, the B–H bond breaking in $\mathbf{INT}_{\text{2-Oo}}$ is by far the preferred mechanism.

To characterize noncovalent interactions (NCIs) that may be driving the precarious stabilization of these intermediates, the NCI analysis of Johnson and co-workers was employed.[76,77] Molecular representations of $\mathbf{INT}^{\text{LA}}_{\text{2-Oo}}$ and $\mathbf{INT}_{\text{2-Oo}}$ with the NCI isosurface are shown in Figure 12. From the molecular representations, it may be seen that both CH/CH and CH/π van der Waals interactions (green surfaces) help favor these transient species. In the $\mathbf{INT}^{\text{LA}}_{\text{2-Oo}}$ system, a strong, attractive interaction (blue) is found between the germanium and oxygen atoms in the Lewis adduct moiety, most probably due to strong Coulombic interactions between Ge and O atoms. Inspection of NBO charges shows a large charge separation between Ge and O with charges 1.30 $|e|$ and -0.84 $|e|$, respectively. On the other hand, for $\mathbf{INT}_{\text{2-Oo}}$, blue surfaces appear in the Ge–H and B–H bonds, revealing highly attractive interactions. Inspection of charges show that the hydride (-0.32 $|e|$) is stabilized electrostatically by the positive charged Ge (1.17 $|e|$) and B (1.20 $|e|$) centers. The Ge–H and B–H bond orders are 0.48 and 0.53, which show the partial formation of these bonds and allowing a total bond order over the hydride of 0.9, which is consistent with a 3c–2e bond.

With the aim of giving a quantitative characterization of the noncovalent interactions, SAPT0 computations[78] were performed on the $\mathbf{INT}^{\text{LA}}_{\text{2-Oo}}$ and $\mathbf{INT}_{\text{2-Oo}}$ species. As summary of the main physical components of the SAPT interaction energies, together with fragmentation used, is shown in Figure 13. The total interaction energies between the fragments for the Lewis and H-bridged intermediates are -38.1 and -35.1 kcal mol^{-1}, respectively. For $\mathbf{INT}^{\text{LA}}_{\text{2-Oo}}$, the main noncovalent interactions are primarily electrostatic, although induction and dispersion also contribute in that order. As a result of the B$\cdots$O bond formation, polarization and charge transfer between fragments can be measured from the induction term. It was found that polarization (-29.6 kcal mol^{-1})

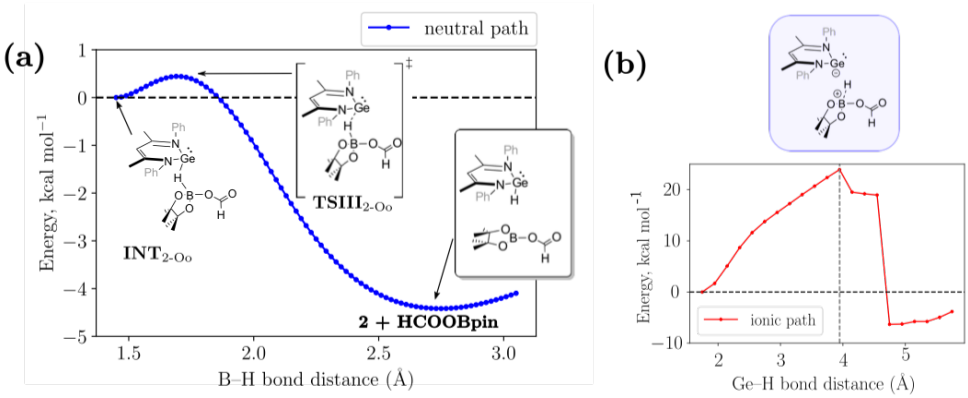

Figure 11: (a) Energy profile along B–H bond distance (neutral path), and (b) energy profile along Ge–H bond (ionic path). For both reaction pathways relevant structures are presented.

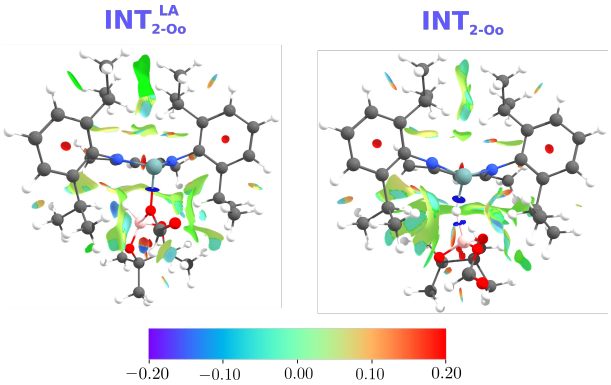

Figure 12: Noncovalent interaction (NCI) analysis of intermolecular interactions in color-code.

is more significant than charge transfer effects (−22.3 kcal mol^{-1}) at this geometry. To study the strong Coulombic interaction revealed by the NCI results, a partition of the Ge–O bond was studied. In this partition, the electrostatic term increases to -135.4 kcal mol^{-1}. For the **INT**$_{2\text{-Oo}}$ species (partition according to Figure 13), induction and dispersion interactions contribute equally to the transient stabilization of this species, with a less pronounced charge transfer energy (−13.6 kcal mol^{-1}) but with higher polarization (−37.7 kcal mol^{-1}). Since the reverse $\Delta G^{\ddagger}_{\text{LA}}$ and the $\Delta G^{\ddagger}_{HB}$ energies are so close for each group 14 center, it is believed that similar intermolecular interactions drive the transient stabilization in the remaining Si, Sn, and Pb-based intermediate.

In summary, in the LA intermediate, the oxygen atom directly attached to Ge transfers electrons to the boron atom in HBpin to form the adduct. This is evidenced with a more substantial electrostatic term and charge transfer energy. Conversely, in the H-bridged intermediate orbital and electrostatic interactions seem to favor the appearance of **INT**$_{2\text{-Oo}}$, but with a diminished electron transfer from the complex to the HCOOBpin moiety through the Ge$\cdots$H$\cdots$B interaction.

Conclusions

The CO_2 activation mechanism by low-valent Si(II), Ge(II), Sn(II), and Pb(II) hydride complexes bearing a bidentated β-diketiminate (NacNac) ligand has been

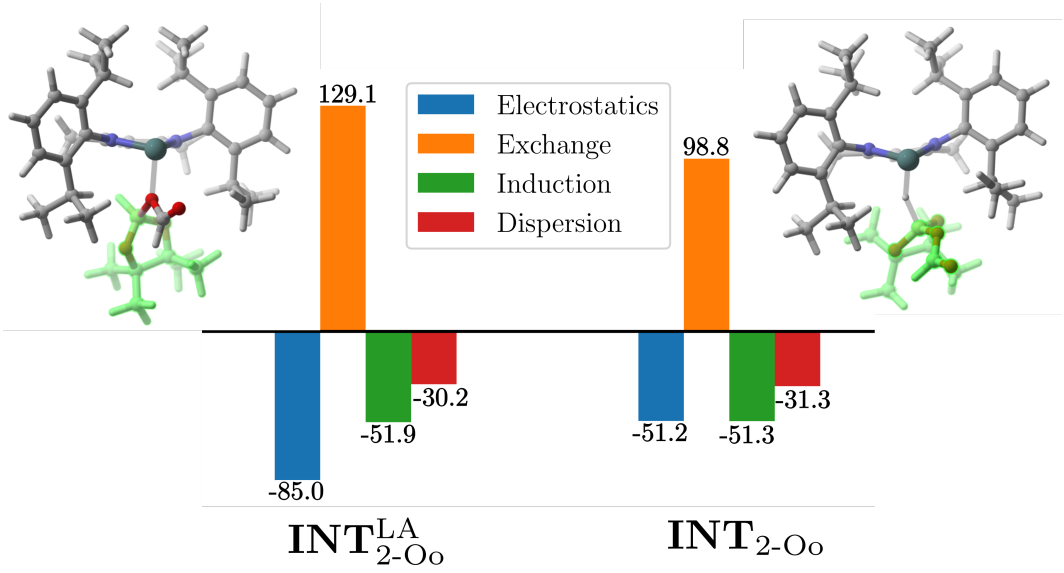

Figure 13: SAPT0 analysis for **INT**$^{LA}_{2\text{-Oo}}$ and **INT**$_{2\text{-Oo}}$ intermediates. Energies are given in kcal mol^{-1}.

studied in great detail by DFT calculations. According to the computed activation energies for whole catalytic cycles, the Pb based complex is predicted to be (by far) the most active towards CO_2 hydroboration, followed in order by the Sn, Ge, and Si analogs: the CO_2 activation and hydroboration processes become more favorable as we descend in group 14. This trend is found as a direct consequence of the enhanced polar character of the **E**–H bond (hydrides) and **E**–O (formates), more Lewis acidic metal center, as the atomic radii of the metal increases when going down in group 14. However, when the catalytic cycle for catalysts **1-4** is compared in energetic terms with the uncatalyzed CO_2+HBpin reaction, an effective energetic decrease is observed from the germanium derivative **2**. Moreover, free energy barriers for the activation and hydroboration of CO_2 from Ge to Pb were found to be low enough –below 22 kcal mol^{-1}– and therefore the process is highly feasible to take place under mild reactions conditions.

Regarding the hydroboration step it was found that only the **PE**H*o* and **PE**O*o* can make possible the hydroboration step, since the *i*-Pr groups in both **PE**H*i* and **PE**O*i* species prevent the approaching of HBpin. Moreover, it has been found that the reaction mechanism for the hydroboration step changes from concerted to stepwise when going down in group 14, with the appearance of two different reaction intermediates: **INT**$^{LA}_{E\text{-Oo}}$ and **INT**$_{E\text{-Oo}}$. From NCI and SAPT computations we showed that in the LA intermediate, the oxygen atom directly attached to Ge transfers electrons to the boron atom in HBpin to form the adduct, which is evidenced with a larger electrostatic term and charge transfer energy. Conversely, in the H-bridged intermediate orbital and electrostatic interactions seem to favor the appearance of **INT**$_{2\text{-Oo}}$ but with a diminished electron transfer from the complex to the HCOOBpin moiety through the Ge$\cdots$H$\cdots$B interaction.

In summary, although an effective catalytic decrease is observed from Ge(II) going down in the group, this computational study suggests the lead(II) hydride complex as a more convenient alternative for activation and hydroboration of CO_2. The trend in reactivity found here should aid in new developments in main group chemistry. Moreover, we have provided computational evidence that a smart choice of the steric demand of the catalyst-hydride source, together with the stoichiometry, may play an essential role in the selective formation of formic and/or methanol intermediates as recently found in TM catalysis.[89] More experimental results are needed to corroborate these findings, but these observations strongly support the intrinsic selectivity power in MG catalysts.

Supporting Information Available

Energy profiles and SAPT along the IRC for the CO_2 activation. Benchmark and NCI plots for $\mathbf{INT}^{\mathrm{LA}}_{\mathrm{E\text{-}Oo}}$ and $\mathbf{INT}_{\mathrm{E\text{-}Oo}}$ intermediates. XYZ coordinates for all systems.

Acknowledgements

Financial support from FONDECYT project no. 1181072 is acknowledged. NVE wishes to acknowledge CONICYT-PCHA/Doctorado Nacional/2016-21161677 and Beca para pasantía en el extranjero CONICYT. Research at the University of Georgia was supported by the United States National Science Foundation, Grant CHE-1661604.

Bibliography

(1) Anderson, D. L. *Theory of the Earth*; Blackwell scientific publications, 1989; Vol. Chapter 8.

(2) Yaroshevsky, A. *Geochemistry International* **2006**, *44*, 48–55.

(3) Hill, M. S.; Liptrot, D. J.; Weetman, C. Alkaline Earths as Main Group Reagents in Molecular Catalysis. *Chem. Soc. Rev.* **2016**, *45*, 972–988.

(4) Power, P. P. Main-Group Elements as Transition Metals. *Nature* **2010**, *463*, 171–177.

(5) Power, P. P. Interaction of Multiple Bonded and Unsaturated Heavier Main Group Compounds with Hydrogen, Ammonia, Olefins, and Related Molecules. *Acc. Chem. Res.* **2011**, *44*, 627–637.

(6) Asay, M.; Jones, C.; Driess, M. N-Heterocyclic Carbene Analogues with Low-Valent Group 13 and Group 14 Elements: Syntheses, Structures, and Reactivities of a New Generation of Multitalented Ligands. *Chem. Rev.* **2010**, *111*, 354–396.

(7) Yao, S.; Xiong, Y.; Driess, M. Zwitterionic and Donor-Stabilized N-Heterocyclic Silylenes (NHSis) for Metal-Free Activation of Small Molecules. *Organometallics* **2011**, *30*, 1748–1767.

(8) Martin, D.; Soleilhavoup, M.; Bertrand, G. Stable Singlet Carbenes as Mimics for Transition Metal Centers. *Chem. Science* **2011**, *2*, 389–399.

(9) Cui, C.; Köpke, S.; Herbst-Irmer, R.; Roesky, H. W.; Noltemeyer, M.; Schmidt, H.-G.; Wrackmeyer, B. Facile Synthesis of Cyclopropene Analogues of Aluminum and an Aluminum Pinacolate, and the Reactivity of LAl[η^2-$C_2(SiMe_3)_2$] toward Unsaturated Molecules (L= HC[(CMe)(NAr)]$_2$, Ar = 2,6-*i*-$Pr_2C_6H_3$). *J. Am. Chem. Soc.* **2001**, *123*, 9091–9098.

(10) Zhu, H.; Chai, J.; Fan, H.; Roesky, H. W.; Nehete, U. N.; Schmidt, H.-G.; Noltemeyer, M. A Rearrangement of Azobenzene upon Interaction with an Aluminum(I) Monomer LAl {L = HC[(CMe)(NAr)]$_2$, Ar = 2,6-*i*$Pr_2C_6H_3$}. *Eur. J. Inorg. Chem.* **2005**, *2005*, 2147–2150.

(11) Zhu, H.; Chai, J.; Fan, H.; Roesky, H. W.; He, C.; Jancik, V.; Schmidt, H.-G.; Noltemeyer, M.; Merrill, W. A.; Power, P. P. A Stable Aluminacyclopropene LAl (η^2-C_2H_2) and Its End-On Azide Insertion to an Aluminaazacyclobutene. *Angew. Chem. Int. Ed.* **2005**, *44*, 5090–5093.

(12) Zhu, H.; Oswald, R. B.; Fan, H.; Roesky, H. W.; Ma, Q.; Yang, Z.; Schmidt, H.-G.; Noltemeyer, M.; Starke, K.; Hosmane, N. S. Aluminacyclopropene: Syntheses, Characterization, and Reactivity toward Terminal Alkynes. *J. Am. Chem. Soc.* **2006**, *128*, 5100–5108.

(13) Jana, A.; Ghoshal, D.; Roesky, H. W.; Objartel, I.; Schwab, G.; Stalke, D. A Germanium (II) Hydride as an Effective Reagent for Hydrogermylation Reactions. *J. Am. Chem. Soc.* **2009**, *131*, 1288–1293.

(14) Jana, A.; Roesky, H. W.; Schulzke, C.; Döring, A. Reactions of Tin (II) Hydride Species with Unsaturated Molecules. *Angew. Chem. Int. Ed.* **2009**, *48*, 1106–1109.

(15) Mandal, S. K.; Roesky, H. W. Group 14 Hydrides with Low Valent Elements for Activation of Small Molecules. *Acc. Chem. Res.* **2011**, *45*, 298–307.

(16) Ganesamoorthy, C.; Bläser, D.; Wölper, C.; Schulz, S. Temperature-Dependent Electron Shuffle in Molecular Group 13/15 Intermetallic Complexes. *Angew. Chem.* **2014**, *126*, 11771–11775.

(17) Ganesamoorthy, C.; Bläser, D.; Wölper, C.; Schulz, S. Sequential Bi–C bond activation reactions of $BiEt_3$ via insertion reactions of RE {R = HC[C(Me)N(2,6−i−$Pr_2C_6H_3$)]$_2$; E = Al, Ga, In}. *Chemical Comm.* **2014**, *50*, 12382–12384.

(18) Chu, T.; Korobkov, I.; Nikonov, G. I. Oxidative addition of σ bonds to an Al (I) center. *J. Am. Chem. Soc.* **2014**, *136*, 9195–9202.

(19) Crimmin, M. R.; Butler, M. J.; White, A. J. Oxidative Addition of Carbon–Fluorine and Carbon–Oxygen bonds to Al (I). *Chem. Comm.* **2015**, *51*, 15994–15996.

(20) Chu, T.; Boyko, Y.; Korobkov, I.; Nikonov, G. I. Transition Metal-like Oxidative Addition of C–F and C–O Bonds to an Aluminum (I) Center. *Organometallics* **2015**, *34*, 5363–5365.

(21) Kong, L.; Ganguly, R.; Li, Y.; Kinjo, R. Serendipitous Observation

of Al^I Insertion into a C–O Bond in L_2PhB (L= Oxazol-2-ylidene). *Chem. Eur. J.* **2016**, *22*, 1922–1925.

(22) Zhang, X.; Cao, Z. Insight into the Reaction Mechanisms for Oxidative Addition of Strong σ Bonds to an Al(I) center. *Dalton Trans.* **2016**, *45*, 10355–10365.

(23) Chu, T.; Boyko, Y.; Korobkov, I.; Kuzmina, L. G.; Howard, J. A.; Nikonov, G. I. Oxidative Addition of Disulfides, Alkyl Sulfides, and Diphosphides to an Aluminum (I) Center. *Inorg. Chem.* **2016**, *55*, 9099–9104.

(24) Protchenko, A. V.; Bates, J. I.; Saleh, L. M.; Blake, M. P.; Schwarz, A. D.; Kolychev, E. L.; Thompson, A. L.; Jones, C.; Mountford, P.; Aldridge, S. Enabling and Probing Oxidative Addition and Reductive Elimination at a Group 14 Metal Center: Cleavage and Functionalization of E–H Bonds by a bis (Boryl) Stannylene. *J. Am. Chem. Soc.* **2016**, *138*, 4555–4564.

(25) Schoeller, W. W.; Frey, G. D. Oxidative Addition of π-bonds and σ-bonds to an Al(I) Center: The Second-Order Carbene Property of the Al-NacNac Compound. *Inorg. Chem.* **2016**, *55*, 10947–10954.

(26) Jakhar, V. K.; Barman, M. K.; Nembenna, S. Aluminum Monohydride Catalyzed Selective Hydroboration of Carbonyl Compounds. *Org. Lett.* **2016**, *18*, 4710–4713.

(27) Li, B.; Kundu, S.; Zhu, H.; Keil, H.; Herbst-Irmer, R.; Stalke, D.; Frenking, G.; Andrada, D. M.; Roesky, H. W. An Open Route to Asymmetric Substituted Al–Al Bonds Using Al(I)- and Al(III)-precursors. *Chem. Comm.* **2017**, *53*, 2543–2546.

(28) Chu, T.; Nikonov, G. I. Oxidative Addition and Reductive Elimination at Main-Group Element Centers. *Chem. Rev.* **2018**, *118*, 3608–3680.

(29) Weetman, C.; Inoue, S. The Road Travelled: After Main-Group Elements as Transition Metals. *ChemCatChem* **2018**, *10*, 4213–4228.

(30) Tuscher, L.; Helling, C.; Wölper, C.; Frank, W.; Nizovtsev, A. S.; Schulz, S. A General Route to Metal-Substituted Dipnictenes of the Type $[L(X)M]_2E_2$. *Chem. Eur. J.* **2018**, *24*, 3241–3250.

(31) Bakewell, C.; White, A. J.; Crimmin, M. R. Reactions of Fluoroalkenes with an Aluminium (I) Complex. *Angew. Chem. Int. Ed.* **2018**, *57*, 6638–6642.

(32) Dai, W.-L.; Luo, S.-L.; Yin, S.-F.; Au, C.-T. The Direct Transformation of Carbon Dioxide to Organic Carbonates over Heterogeneous Catalysts. *Applied Catalysis A: General* **2009**, *366*, 2–12.

(33) Tsuji, Y.; Fujihara, T. Carbon Dioxide as a Carbon Source in Organic Transformation: Carbon–Carbon Bond Forming reactions by Transition-Metal Catalysts. *Chem. Comm.* **2012**, *48*, 9956–9964.

(34) Das Neves Gomes, C.; Jacquet, O.; Villiers, C.; Thuéry, P.; Ephritikhine, M.; Cantat, T. A Diagonal Approach to Chemical Recycling of Carbon Dioxide: Organocat-

alytic Transformation for the Reductive Functionalization of CO_2. *Angew. Chem. Int. Ed.* **2012**, *51*, 187–190.

(35) Tan, G.; Wang, W.; Blom, B.; Driess, M. Mechanistic Studies of CO_2 Reduction to Methanol Mediated by an N-Heterocyclic Germylene Hydride. *Dalton Trans.* **2014**, *43*, 6006–6011.

(36) Hadlington, T. J.; Hermann, M.; Frenking, G.; Jones, C. Low Coordinate Germanium(II) and Tin(II) Hydride Complexes: Efficient Catalysts for the Hydroboration of Carbonyl Compounds. *J. Am. Chem. Soc.* **2014**, *136*, 3028–3031.

(37) Hadlington, T. J.; Kefalidis, C. E.; Maron, L.; Jones, C. Efficient Reduction of Carbon Dioxide to Methanol Equivalents Catalyzed by Two-Coordinate Amido–Germanium(II) and -Tin(II) Hydride Complexes. *ACS Catal.* **2017**, *7*, 1853–1859.

(38) Jana, A.; Sen, S. S.; Roesky, H. W.; Schulzke, C.; Dutta, S.; Pati, S. K. End-On Nitrogen Insertion of a Diazo Compound into a Germanium(II) Hydrogen Bond and a Comparable Reaction with Diethyl Azodicarboxylate. *Angew. Chem. Int. Ed.* **2009**, *48*, 4246–4248.

(39) Jana, A.; Tavčar, G.; Roesky, H. W.; John, M. Germanium(II) Hydride Mediated Reduction of Carbon Dioxide to Formic Acid and Methanol with Ammonia Borane as the hydrogen Source. *Dalton Trans.* **2010**, *39*, 9487–9489.

(40) Jana, A.; Roesky, H. W.; Schulzke, C. Reactivity of Germanium(II) Hydride with Nitrous Oxide, Trimethylsilyl Azide, Ketones, and Alkynes and the Reaction of a Methyl Analogue with Trimethylsilyl Diazomethane. *Dalton Trans.* **2010**, *39*, 132–138.

(41) Mandal, S. K.; Roesky, H. W. Group 14 Hydrides with Low Valent Elements for Activation of Small Molecules. *Acc. Chem. Res.* **2011**, *45*, 298–307.

(42) Jambor, R.; Lyčka, A. Organosilicon and -Germanium Hydrides in Catalyst-Free Hydrometallation Reactions. *Eur. J. Inor. Chem.* **2017**, *2017*, 4887–4898.

(43) Aldridge, S.; Downs, A. J. Hydrides of the Main-Group Metals: New Variations on an Old Theme. *Chem. Rev.* **2001**, *101*, 3305–3366.

(44) McGrady, G. S.; Guilera, G. The Multifarious World of Transition Metal Hydrides. *Chem. Soc. Rev.* **2003**, *32*, 383–392.

(45) Zhao, J.; Goldman, A. S.; Hartwig, J. F. Oxidative Addition of Ammonia to Form a Stable Monomeric Amido Hydride Complex. *Science* **2005**, *307*, 1080–1082.

(46) Mueller, W. M.; Blackledge, J. P.; Libowitz, G. G. *Metal hydrides*; Elsevier, 2013.

(47) Rivard, E. Group 14 Inorganic Hydrocarbon Analogues. *Chem. Soc. Rev.* **2016**, *45*, 989–1003.

(48) Villegas-Escobar, N.; Ortega, D. E.; Cortés-Arriagada, D.; Duran, R.; Yepes, D.; Gutierrez-Oliva, S.; Toro-Labbé, A. Why Low Valent Lead (II)

Hydride Complex Would be a Better Catalyst for CO_2 Activation than Its 14 Group Analogues? *J. Phys. Chem. C* **2017**, *121*, 12127–12135.

(49) Wartik, T.; Pearson, R. Reactions of Carbon Dioxide with Sodium and Lithium Borohydrides. *J.Inorg. Nucl. Chem.* **1958**, *7*, 404–411.

(50) Knopf, I.; Cummins, C. C. Revisiting CO2 Reduction with NaBH4 under aprotic conditions: Synthesis and characterization of sodium triformatoborohydride. *Organometallics* **2015**, *34*, 1601–1603.

(51) Légaré, M.-A.; Courtemanche, M.-A.; Fontaine, F.-G. Lewis Base Activation of Borane–Dimethylsulfide into Strongly Reducing Ion Pairs for the Transformation of Carbon Dioxide to Methoxyboranes. *Chem. Comm.* **2014**, *50*, 11362–11365.

(52) Lafage, M.; Pujol, A.; Saffon-Merceron, N.; Milles, N. BH_3 Activation by Phosphorus-Stabilized Geminal Dianions: Synthesis of Ambiphilic Organoborane, DFT Studies, and Catalytic CO_2 Reduction into Methanol Derivatives. *ACS Catal.* **2016**, *6*, 3030–3035.

(53) Ho, S. Y.-F.; So, C.-W.; Saffon-Merceron, N.; Mézailles, N. Formation of a Zwitterionic Boronium Species from the Reaction of a Stable Carbenoid with Borane: CO_2 Reduction. *Chem. Comm.* **2015**, *51*, 2107–2110.

(54) Courtemanche, M.-A.; LrM.-A.; Maron, L.; Fontaine, F.-G. A Highly Active Phosphine–Borane Organocatalyst for the Reduction of CO_2 to Methanol using Hydroboranes. *J. Am. Chem. Soc.* **2013**, *135*, 9326–9329.

(55) Wang, T.; Stephan, D. W. Carbene-9-BBN Ring Expansions as a Route to Intramolecular Frustrated Lewis Pairs for CO_2 Reduction. *Chem. Eur. J.* **2014**, *20*, 3036–3039.

(56) Yang, Y.; Xu, M.; Song, D. Organocatalysts with Carbon-Centered Activity for CO_2 Reduction with Boranes. *Chem. Comm.* **2015**, *51*, 11293–11296.

(57) Ramos, A.; Antiñolo, A.; Carrillo-Hermosilla, F.; Fernández-Galán, R.; Rodríguez-Diéguez, A.; García-Vivó, D. Carbodiimides as Catalysts for the Reduction of CO_2 with Boranes. *Chem. Comm.* **2018**, *54*, 4700–4703.

(58) Yang, Y.; Yan, L.; Xie, Q.; Liang, Q.; Song, D. Zwitterionic Indenylammonium with Carbon-Centred Reactivity Towards Reversible CO_2 Binding and Catalytic Reduction. *Org. Biomol. Chem.* **2017**, *15*, 2240–2245.

(59) Sau, S. C.; Bhattacharjee, R.; Vardhanapu, P. K.; Vijaykumar, G.; Datta, A.; Mandal, S. K. Metal-Free Reduction of CO_2 to Methoxyborane under Ambient Conditions through Borondiformate Formation. *Angew. Chem. Int. Ed.* **2016**, *55*, 15147–15151.

(60) Declercq, R.; Bouhadir, G.; Bourissou, D.; LrM.-A.; Courtemanche, M.-A.; Nahi, K. S.; Bouchard, N.; Fontaine, F.-G.; Maron, L. Hydroboration of Carbon Dioxide Using Ambiphilic Phosphine–Borane Catalysts: On the Role of the Formalde-

hyde Adduct. *ACS Catal.* **2015**, *5*, 2513–2520.

(61) Takagi, N.; Sakaki, S. Theoretical Study of Reactivity of Ge(II)-Hydride Compound: Comparison with Rh(I)-Hydride Complex and Prediction of Full Catalytic Cycle by Ge(II)-Hydride. *J. Am. Chem. Soc.* **2013**, *135*, 8955–8965.

(62) Zhao, Y.; Truhlar, D. G. The M06 Suite of Density Functionals for Main Group Thermochemistry, Thermochemical Kinetics, Noncovalent Interactions, Excited States, and Transition Elements: Two New Functionals and Systematic Testing of Four M06-Class Functionals and 12 other Functionals. *Theor. Chem. Acc.* **2008**, *120*, 215–241.

(63) Dill, J. D.; Pople, J. A. Self-Consistent Molecular Orbital Methods. XV. Extended Gaussian-type Basis Sets for Lithium, Beryllium, and Boron. *J. Chem. Phys.* **1975**, *62*, 2921–2923.

(64) Francl, M. M.; Pietro, W. J.; Hehre, W. J.; Binkley, J. S.; Gordon, M. S.; Drefrees, D. J.; Pople, J. A. Self-Consistent Molecular Orbital Methods. XXIII. A Polarization-type Basis Set for Second-Row Elements. *J. Chem. Phys.* **1982**, *77*, 3654–3665.

(65) Zhao, Y.; Truhlar, D. G. Exploring the Limit of Accuracy of the Global Hybrid Meta Density Functional for Main-Group Thermochemistry, Kinetics, and Noncovalent Interactions. *J. Chem. Theory Comput.* **2008**, *4*, 1849–1868.

(66) Valero, R.; Costa, R.; de PR Moreira, I.; Truhlar, D. G.; Illas, F. Performance of the M06 Family of Exchange-Correlation Functionals for Predicting Magnetic Coupling in Organic and Inorganic Molecules. *J. Chem. Phys.* **2008**, *128*, 114103.

(67) Hay, P. J.; Wadt, W. R. Ab Initio Effective Core Potentials for Molecular Calculations. Potentials for K to Au Including the Outermost Core Orbitals. *J. Chem. Phys.* **1985**, *82*, 299–310.

(68) Scott, A. P.; Radom, L. Harmonic Vibrational Frequencies: An Evaluation of Hartree-Fock, Mϕller-Plesset, Quadratic Configuration Interaction, Density Functional Theory, and Semiempirical Scale Factors. *J. Phys. Chem.* **1996**, *100*, 16502–16513.

(69) Fukui, K. The Path of Chemical Reactions-The IRC Approach. *Acc. Chem. Res.* **1981**, *14*, 363–368.

(70) Hratchian, H. P.; Schlegel, H. B. Accurate Reaction Paths Using a Hessian Based Predictor-Corrector Integrator. *J. Chem. Phys.* **2004**, *120*, 9918–9924.

(71) Hratchian, H. P.; Schlegel, H. B. Using Hessian Updating to Increase the Efficiency of a Hessian Based Predictor-Corrector Reaction Path Following Method. *J. Chem. Theory and Comp.* **2005**, *1*, 61–69.

(72) Grimme, S. *Chem. Eur. J.* **2012**, *18*, 9955–9964.

(73) Tomasi, J.; Mennucci, B.; Cammi, R. Quantum Mechanical Continuum Solvation Models. *Chem. Rev.* **2005**, *105*, 2999–3094.

(74) Frisch, M. J. et al. Gaussian 09 Revision B.01. *Gaussian Inc. Wallingford CT 2009*

(75) Reed, A. E.; Curtiss, L. A.; Weinhold, F. Intermolecular Interactions from a Natural Bond Orbital, Donor-Acceptor Viewpoint. *Chem. Rev.* **1988**, *88*, 899–926.

(76) Johnson, E. R.; Keinan, S.; Mori-Sanchez, P.; Contreras-Garcia, J.; Cohen, A. J.; Yang, W. Revealing Noncovalent Interactions. *J. Am. Chem. Soc.* **2010**, *132*, 6498–6506.

(77) Contreras-García, J.; Johnson, E. R.; Keinan, S.; Chaudret, R.; Piquemal, J.-P.; Beratan, D. N.; Yang, W. *J. Chem. Theory Comput.* **2011**, *7*, 625–632.

(78) Jeziorski, B.; Moszynski, R.; Szalewicz, K. Perturbation Theory Approach to Intermolecular Potential Energy Surfaces of Van der Waals Complexes. *Chem. Rev.* **1994**, *94*, 1887–1930.

(79) Stone, A. J. Computation of Charge-Transfer Energies by Perturbation Theory. *Chem. Phys. Lett.* **1993**, *211*, 101–109.

(80) Khaliullin, R. Z.; Cobar, E. A.; Lochan, R. C.; Bell, A. T.; Head-Gordon, M. Unravelling the Origin of Intermolecular Interactions Using Absolutely Localized Molecular Orbitals. *J. Phys. Chem. A* **2007**, *111*, 8753–8765.

(81) Stone, A. J.; Misquitta, A. J. Charge-Transfer in Symmetry-Adapted Perturbation Theory. *Chem. Phys. Lett.* **2009**, *473*, 201–205.

(82) Misquitta, A. J. Charge Transfer from Regularized Symmetry-Adapted Perturbation Theory. *J. Chem. Theory Comput.* **2013**, *9*, 5313–5326.

(83) Parrish, R. M. et al. Psi4 1.1: An Open-Source Electronic Structure Program Emphasizing Automation, Advanced Libraries, and Interoperability. *J. Chem. Theory Comput.* **2017**, *13*, 3185–3197.

(84) Hohenstein, E. G.; Sherrill, C. D. Density Fitting and Cholesky Decomposition Approximations in Symmetry-Adapted Perturbation Theory: Implementation and Application to Probe the Nature of $\pi - \pi$ Interactions in Linear Acenes. *J. Chem. Phys.* **2010**, *132*, 184111.

(85) Hohenstein, E. G.; Parrish, R. M.; Sherrill, C. D.; Turney, J. M.; Schaefer III, H. F. Large-Scale Symmetry-Adapted Perturbation Theory Computations via Density Fitting and Laplace Transformation Techniques: Investigating the Fundamental Forces of DNA-Intercalator Interactions. *J. Chem. Phys.* **2011**, *135*, 174107.

(86) Westcott, S. A.; Blom, H. P.; Marder, T. B.; Baker, R. T.; Calabrese, J. C. Nucleophile Promoted Degradation of Catecholborane: Consequences for Transition Metal-Catalyzed Hydroborations. *Inorg. Chem.* **1993**, *32*, 2175–2182.

(87) Stoelzel, M.; Präsang, C.; Inoue, S.; Enthaler, S.; Driess, M. Hydrosilylation of Alkynes by $Ni(CO)_3$-Stabilized Silicon(II) Hydride. *Angew. Chem. Int. Ed.* **2012**, *51*, 399–403.

(88) Jungton, A.-K.; Meltzer, A.; Präsang, C.; Braun, T.; Driess, M.; Penner, A. Addition of [(η^5-C_5Me_5)IrH_4] to a Zwitterionic Silylene: Stepwise Formation of Iridium(V)-Silyl and Iridium(III)-Silylene Complexes. *Dalton Trans.* **2010**, *39*, 5436–5438.

(89) Espinosa, M. R.; Charboneau, D. J.; Garcia de Oliveira, A.; Hazari, N. Controlling Selectivity in the Hydroboration of Carbon Dioxide to the Formic Acid, Formaldehyde, and Methanol Oxidation Levels. *ACS Catal.* **2018**, *9*, 301–314.

(90) Chen, M.; Fulton, J. R.; Hitchcock, P. B.; Johnstone, N. C.; Lappert, M. F.; Protchenko, A. V. Synthesis and Theoretical Studies on Rare Three-Coordinate Lead Complexes. *Dalton Trans.* **2007**, 2770–2778.

(91) Fulton, J. R.; Hitchcock, P. B.; Johnstone, N. C.; Tam, E. C. The Synthesis of Monomeric Terminal Lead Aryloxides: Dependence on Reagents and conditions. *Dalton Trans.* **2007**, 3360–3362.

(92) Yao, S.; Block, S.; Brym, M.; Driess, M. A New Type of Heteroleptic Complex of Divalent Lead and Synthesis of the P-plumbyleniophosphasilene, $R_2Si{=}P{-}Pb(L)$: (L = β-diketiminate). *Chem. Comm.* **2007**, 3844–3846.

(93) Tam, E. C.; Johnstone, N. C.; Ferro, L.; Hitchcock, P. B.; Fulton, J. R. Carbon Dioxide Activation by "non-nucleophilic" Lead Alkoxides. *Inorg. Chem.* **2009**, *48*, 8971–8976.

(94) Tam, E. C.; Coles, M. P.; Smith, J. D.; Fulton, J. R. The Steric Influence of β-diketiminato Ligands on the Coordination Chemistry of Lead(II). *Polyhedron* **2015**, *85*, 284–294.

(95) Jana, A.; Sarish, S. P.; Roesky, H. W.; Schulzke, C.; Döring, A.; John, M. Facile Access of Well-Defined Stable Divalent Lead Compounds with Small Organic Substituents. *Organometallics* **2009**, *28*, 2563–2567.

(96) Harris, L. A.-M.; Tam, E. C.; Coles, M. P.; Fulton, J. R. Lead and Tin β-diketiminato Amido/Anilido Complexes: Competitive Nucleophilic Reactivity at the β-diketiminato γ-carbon. *Dalton Trans.* **2014**, *43*, 13803–13814.

(97) Schneider, J.; Sindlinger, C. P.; Eichele, K.; Schubert, H.; Wesemann, L. Low-Valent Lead Hydride and Its Extreme Low-Field ^{1}H-NMR Chemical Shift. *J. Am. Chem. Soc.* **2017**, *139*, 6542–6545.

(98) Queen, J. D.; Fettinger, J. C.; Power, P. P. Two quasi-Stable Lead(II) Hydrides at Ambient Temperature. *Chem. Comm.* **2019**, *55*, 10285–10287.

Graphical TOC Entry